On the Transition from Radiating to Guiding Behavior of the Half-Mode Substrate Integrated Waveguide

Qinghua Lai [#1], Christophe Fumeaux [*2], Wei Hong [#3]

[#] *State Key Laboratory of Millimeter Waves, School of Information Science and Engineering*
Southeast University, Nanjing, 210096, P. R. China
[1]*qhlai@emfield.org*, [3]*weihong@seu.edu.cn*
[*] *School of Electrical and Electronic Engineering, The University of Adelaide*
Adelaide, South Australia 5005
[2]*cfumeaux@eleceng.adelaide.edu.au*

***Abstract* — The transition from radiative to guiding behavior of a half-mode substrate integrated waveguide (HMSIW) is studied throughout this work. The electric near-field distribution in the substrate plane is first demonstrated at different frequencies over the mono-mode operation band and is then related to far-field radiation patterns. The observation shows that the HMSIW, as a semi-open transmission line, suffers from relatively large radiation loss as it operates at frequencies just above the cut-off. However, the radiated power drops drastically with the increase of frequency. In particular, the attenuation caused by radiation becomes negligible as the frequency increases beyond a critical point. An explanation is given to the phenomena above and an approximate equation is also proposed for estimating the critical frequency point, as low-frequency limit of the HMSIW operational range. These results provide a physical confirmation of the optimal operation frequency range for the use of HMSIW as a low-loss waveguide.**

***Index Terms* — Half-mode substrate integrated waveguide, radiation loss**

I. INTRODUCTION

Due to the existence of open side, a half-mode substrate integrated waveguide (HMSIW) generally exhibits relatively large power leakage as it operates near its cutoff frequency [1]. However, as the frequency increases over a critical point, the radiation loss rapidly decreases to become a secondary cause for the overall attenuation. It has been demonstrated that, at mm-wave frequencies, the HMSIW can exhibit lower attenuation constant than a corresponding microstrip line and substrate integrated waveguide (SIW) [1].

In the present paper, the radiation behavior of the HMSIW is described from two different complementary aspects. Firstly, images of the simulated field distribution in the substrate plane (inside and outside the waveguide) are presented at different frequency points to give a good intuition on the physics of radiation. Secondly the far-field radiation patterns broadside from the HMSIW are demonstrated. A theoretical analysis is conducted to explain those observations. In this study, a particular focus is to confirm the existence of a critical frequency point, above which radiation from the HMSIW is reduced to a significantly low level consistent with low-loss guided propagation. An approximate formula is deduced for estimation of that frequency value. The frequency range counted from that frequency point to $3f_c$ is considered optimal for the use of HMSIW as a low-loss transmission line.

II. MODEL

Fig. 1 (a) and (b) show sketches of the 3D and front view configurations of an HMSIW. Fig. 1(c) plots the structure of the HMSIW model that is used in the commercial electromagnetic simulation software HFSS^{TM}. The substrate area as well as the ground plane is extended far outside the HMSIW open side, to provide a better view of the electric

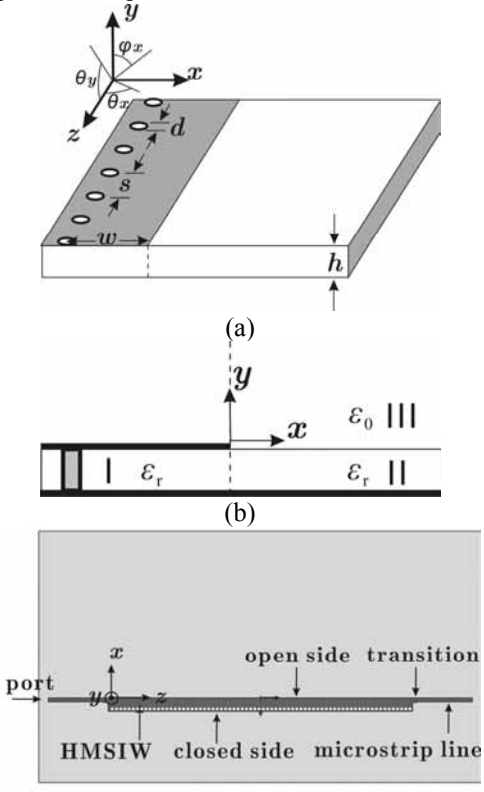

Fig. 1 Sketch of an HMSIW. (a) 3D view; (b) cross-section, and (c) the HMSIW model used in HFSS^{TM}.

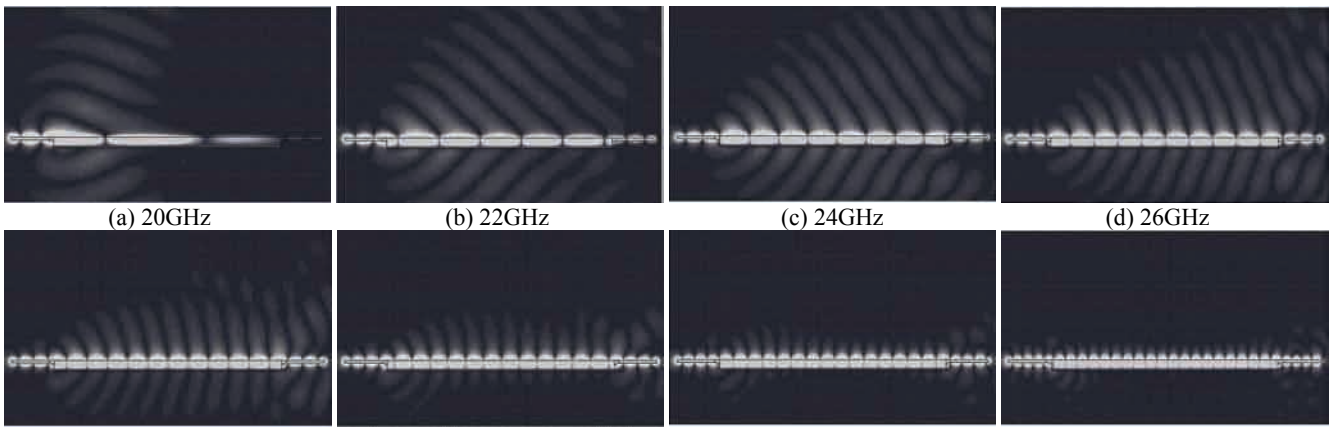

(a) 20GHz (b) 22GHz (c) 24GHz (d) 26GHz

(e) 28GHz (f) 30GHz (g) 34GHz (h) 40GHz

Fig.2 Simulated electric field distributions in the substrate plane (xz plane) at different frequencies. The electric field is plotted on a saturated scale of 0-2000 V/m, which represents a fraction of the maximum field of 44000 V/m in the waveguide.

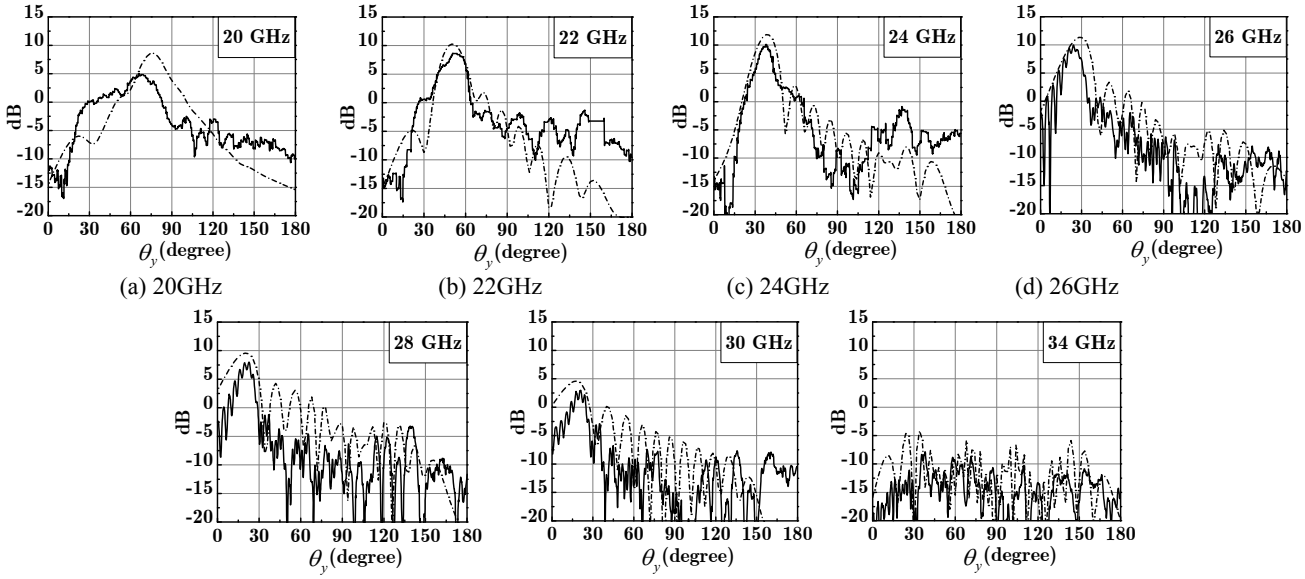

(a) 20GHz (b) 22GHz (c) 24GHz (d) 26GHz

(e) 28GHz (f) 30GHz (g) 34GHz

Fig.3 Simulated and measured radiation patterns at different frequencies, in the yz plane above the HMSIW plane. Dashed lines correspond to the simulation results and solid lines to the measurement results.

field distribution in the grounded dielectric slab. Furthermore, to allow the connection of fabricated prototypes to the measurement apparatus through coaxial connectors, two segments of 50 Ω standard microstrip lines are applied to feed the HMSIW at both ends, as shown in Fig. 1(c). This also eases the assignment of ports in the simulation tool. A tapered microstrip transition with optimized length of 1.2 mm and width of 1.1 mm is additionally inserted between the feeding microstrip line and the HMSIW for impedance matching. The HMSIW is designed with a cut-off frequency f_c = 20.0 GHz. It has a width w = 2.5 mm and a height h = 0.254 mm. The diameter of the metallic vias is d = 0.5 mm and the spacing between them is s = 0.6 mm. The substrate is made of Rogers 5880 dielectric material with a relative permittivity of 2.2 and a loss tangent of 0.001 at 10 GHz.

III. ELECTRIC FIELD DISTRIBUTION AND RADIATION PATTERNS

A. Electric Field Distribution in the Substrate Plane

Fig. 2 illustrates the instantaneous simulated electric field distribution in the substrate plane (xz-plane) at different frequency points. The range of the grayscale plots is reduced to 0 – 2000 V/m, as compared to the full range of 0 – 44000 V/m that is automatically provided by HFSS™. This modification of the range benefits the observation of the fields outside the HMSIW but results in a saturated scale for the fields inside the waveguide. Fig. 2(a) shows that the radiated mode in the substrate travels in a direction near perpendicular to the HMSIW at 20.0 GHz. With the frequency increasing, the propagation direction gradually gets inclined towards the forward propagation direction of

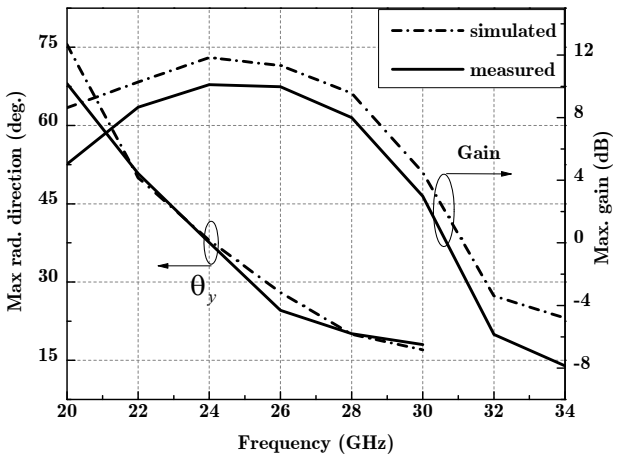

Fig. 4 The maximum gain and the pointing direction of the main beam as a function of frequency.

the waveguide, i.e. the +z direction (see Fig. 2(b)-(d)). Furthermore, the radiating mode amplitude rapidly decreases with the increase of frequency. As a result, the fields nearly become invisible in the applied scale in the exterior substrate at frequencies above 34.0 GHz (Fig. 2 (g) and (h)).

B. Radiation Patterns

Fig. 3 presents the simulated and measured radiation patterns in the yz plane above the HMSIW at the frequency points corresponding to those of Fig. 2. Significant power leakage is observed in the frequency range from 20.0 to 30.0 GHz, where the main beam scans from nearly broadside to the forward end-fire of the HMSIW. As the frequency reaches 34.0 GHz, the measured maximum gain decreases to about -10 dB and the main lobe cannot be distinguished any more. Fig. 4 plots the maximum gain and pointing direction of the main lobe as a function of frequency. The measurement results show that with the frequency rising from 20.0 GHz to 30.0 GHz, the main beam scans from θ_y = 68.0° to θ_y = 18.0°, where θ_y is the angle counted from the +*z* axis to the main beam as defined in Fig. 1(a). At frequencies above 30.0 GHz, the main beam vanishes, making the angle θ_y no longer measurable. Correspondingly, the gain also exhibits a significant value at frequencies below 30.0 GHz with the maximum value of 10.0 dB at around 25.0 GHz. For frequencies above 30.0 GHz, the measured gain quickly decreases with its value reaching -8.0 dB at 34.0 GHz.

IV. INTERPRETATION

This section provides a physical explanation of the HMSIW radiation behavior. As shown in Fig. 1(b), the whole structure composed of the HMSIW and its surrounding materials is divided into three sub-regions. The first region (denoted as I) is the HMSIW interior and the second one (II) is the substrate volume exterior to the waveguide. The free space above the substrate is the third zone (III). Wave numbers of the modes existing in these three regions are

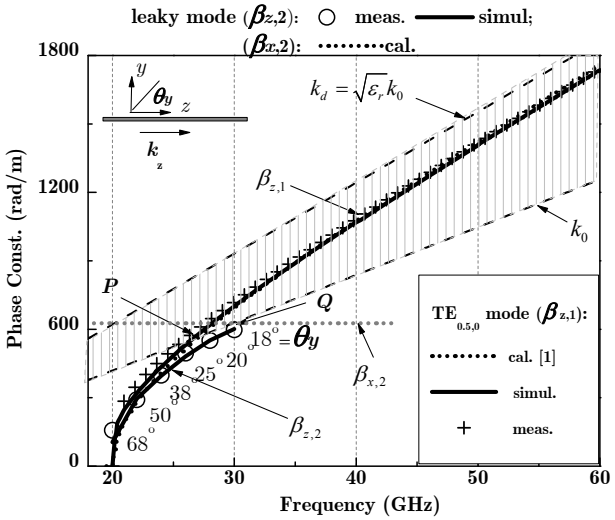

Fig. 5 Phase constants of the fundamental quasi-$TE_{0.5,0}$ mode in the HMSIW and the corresponding leaky-mode excited by the HMSIW.

assumed in the form of $k_{m,i} = \beta_{m,i} - j\alpha_{m,i}$ with $\beta_{m,i}$ and $\alpha_{m,i}$ being the phase constant and attenuation constant, respectively. The subscript m ($m = x, y, z$) represents the axis and the subscript i ($i = 1, 2, 3$) denotes the region. Obviously, the parameter $k_{z,1} = \beta_{z,1} - j\alpha_{z,1}$ corresponds to the z-axis wave number of the dominant quasi-$TE_{0.5,0}$ mode inside the HMSIW. Fig. 5 plots the curves of $\beta_{z,1}$ for the HMSIW model with dimensions given in Section II. The simulated and measured data are gained by using the multiline method [2] and the calculated results are obtained from the formulas developed in [Eq. (12), 1]. A shadow area is also highlighted in this graph with its lower and upper boundaries formed by curves of $\beta = k_0$ and $\beta = \sqrt{\varepsilon_r} k_0$, respectively, where $k_0 = 2\pi f / c$ is the wave number in free space with f and c being the frequency and free-space light velocity, respectively. Any mode with its phase constant β located in that the curve of $\beta_{z,1}$ is below that of $\beta = \sqrt{\varepsilon_r} k_0$ over the this region is bounded in the substrate and does not radiates energy into the upper half-space [3, pp. 163-168]. Fig.6 shows that the curve of $\beta_{z,1}$ is below that of $\beta = \sqrt{\varepsilon_r} k_0$ over the entire frequency range, therefore, the quasi-$TE_{0.5,0}$ mode leaks from the HMSIW open side into the outer grounded substrate slab at any frequency [4]. The angle θ_x of maximum radiation (as defined in Fig. 1) is calculated as [3, pp. 143-148]

$$\tan\theta_x = \frac{\beta_{x,2}}{\beta_{z,2}}. \qquad (1)$$

where $\beta_{x,2}$ and $\beta_{z,2}$ are phase constants of the leaked mode in Region II along the x- and z-axes, respectively. According to the continuous boundary condition satisfied by the wave numbers at the interface of Region I and II, the values of phase constants $\beta_{x,2}$ and $\beta_{z,2}$ can be estimated at $\beta_{x,2} \simeq \beta_{x,1} = \pi / 2w$ [Eq.(3), 1] and $\beta_{z,2} \simeq \beta_{z,1}$, respectively.

As the frequency increases above the cut-off frequency f_c, $\beta_{x,2}$ nearly remains constant but $\beta_{z,2}$ monotonously rises upwards from zero as shown in Fig. 5. That causes the incident angle θ_x to gradually decrease from 90° to an angle approaching zero according to (1). This effect is clearly visible in Fig. 2(a)-(e). Moreover, the amplitude of the radiated wave decreases very quickly in the substrate region beyond the angle of θ_x. That explains why the fields become nearly invisible in the outer substrate at 40 GHz, as the radiated wave travels forwards with the maximum at a relatively small angle θ_x.

The far-field radiation behavior above the HMSIW plane is investigated in the remaining part of this section. It is well known that only when a mode is a fast wave ($\beta_{z,2} < k_0$), it can radiate into the upper half-space with the main lobe pointing in the direction as determined by [4]

$$\sin\theta_y = \frac{\beta_{z,2}}{k_0} \qquad (2)$$

where the angle θ_y of maximal radiation is as defined in Fig. 1(a). Fig. 5 plots the curve of $\beta_{z,2}$ obtained using (2) through inverse calculation based on the measured pointing direction of the main beam as represented in Fig. 4. It shows that the curve of $\beta_{z,2}$ is very close to that of $\beta_{z,1}$ especially at frequencies near the cut-off. Therefore, considering the difficulty in the calculation of $\beta_{z,2}$, one can in practice calculate the value of $\beta_{z,1}$ and use $\beta_{z,2} \simeq \beta_{z,1}$ to substitute it into (2) for estimating the pointing direction θ_y of the main lobe. The small difference between $\beta_{z,1}$ and $\beta_{z,2}$ can be explained as follows. Wave numbers of the quasi-$TE_{0.5,0}$ mode inside the HMSIW and of the leaky mode in the outer substrate volume satisfy the following separation equation [3, pp. 143-148]

$$k_{x,i}^2 + k_{y,i}^2 + k_{z,i}^2 = \varepsilon_r k_0^2 \qquad \text{for } i = 1, 2 . \qquad (3)$$

Rearrangement of (3) leads to

$$\beta_{z,i} \simeq k_{z,i} = \sqrt{\varepsilon_r k_0^2 - (k_{x,i}^2 + k_{y,i}^2)} \qquad \text{for } i = 1, 2 \qquad (4)$$

where the attenuation constant $\alpha_{z,i}$ of $k_{z,i}$ is assumed small enough to be omitted. In the case of $i = 1$, the value of $k_{y,1}$ is close to zero for the dominant quasi-$TE_{0.5,0}$ mode traveling inside the HMSIW. But in the case of $i = 2$, the value of $k_{y,2}$ is *non-zero* since the mode leaks into the upper half-space. With the relations of $k_{x,1} \simeq k_{x,2}$, $k_{y,1} \to 0$ and $k_{y,2} > 0$, (4) leads to $\beta_{z,1} > \beta_{z,2}$. That also explains why the intersection frequency point f_P between curves of $\beta_{z,1}$ and $\beta = k_0$ is lower than that f_Q of $\beta_{z,2}$ and $\beta = k_0$, as shown in Fig. 6. By setting $k_{z,1} = k_0$ in (3), the value of f_P can be calculated as

$$f_P = \frac{c}{2\pi}\sqrt{\frac{k_{x,1}^2 + k_{y,1}^2}{\varepsilon_r - 1}} \approx f_c\sqrt{\frac{\varepsilon_r}{\varepsilon_r - 1}} , \qquad (4)$$

in which $k_{x,1}$ is computed as [Eq.(3), 1] and $k_{y,1}$ is approximately set as zero. As for the value of f_Q, it is empirically found 5-15% above f_P, i.e. $f_Q = (1.05 - 1.15) f_P$, through numerous computed cases.

Fig. 5 further shows that at frequencies above f_Q, the relations of $\beta_{x,2} < k_0$ (fast wave) and $\beta_{z,2} > k_0$ (slow wave) exist. Therefore, the mode in the outer substrate still radiates into the upper half-space with its main lobe theoretically scanning in the xz-plane. However, the resulting radiation loss is significantly reduced as compared to that at frequencies below f_Q because of the decreased fields radiated into the substrate, as observed in Fig. 2(f). It is further empirically found that beyond a critical frequency point around $(1.1 - 1.4) f_Q$, the radiation loss is reduced to a level as low as compatible with practical use of the HMSIW as a waveguide [Fig. 9, 1]. The exact value of that critical point depends on the substrate permittivity, the waveguide width-to-height ratio and the amount of radiation loss that can be tolerated. The frequency range from this point to $3 f_c$ (the upper limit for the mono-mode operation) is regarded as optimal for the HMSIW used as a low insertion loss waveguide. At frequencies below f_Q, the HMSIW can be designed for use as leaky wave antenna [5].

V. Conclusion

The frequency-dependent transition from radiative to guiding behavior of the half-mode substrate integrated waveguide has been investigated in this work. The study shows that there exists a critical point in the frequency domain, above which the HMSIW can operate as waveguide with insignificant radiation loss, but below which the HMSIW functions similarly to a uniform leaky wave antenna [5]. An approximate equation is provided for determining that critical frequency point.

References

[1] Q. H. Lai, C. Fumeaux, W. Hong, and R. Vahldieck, "Characterization of the propagation properties of the half-mode substrate integrated waveguide," *IEEE Trans. Microw. Theory Tech*., vol. 57, no. 8, pp. 1996-2004, Aug. 2009.

[2] R. B. Marks, "A multiline method of network analyzer calibration," *IEEE Trans. Microw. Theory Tech*., vol. 39, pp. 1205-1215, July 1991.

[3] R. F. Harrington, *Time-Harmonic Electromagnetic Field*. New York: McGraw-Hill, 1961, pp. 143-148 & pp. 163-168.

[4] C. A. Balanis. *Modern Antenna Handbook*. New Jersey: John Wiley & Sons, Inc, 2008. 325-367.

[5] J. Xu, W. Hong, H. Tang, Z. Kuai, K. Wu, "Half-Mode Substrate Leaky-Wave Antenna for Millimeter-Wave Applications," *IEEE Antennas and Wireless Propaga. Lett.*, vol. 7, pp 85-88, 2008.